# BaF radical: A promising candidate for laser cooling and magneto-optical trapping*

Liang Xu(许亮), Bin Wei(魏斌), Yong Xia(夏勇), Lian-Zhong Deng(邓联忠), and Jian-Ping Yin(印建平)†

*State Key Laboratory of Precision Spectroscopy, School of Physics and Materials Science, East China Normal University, Shanghai* 200062, *China*

(Received 10 November 2016; revised manuscript received 7 December 2016; published online 13 February 2017)

Recently, there have been great interest and advancement in the field of laser cooling and magneto-optical trapping of molecules. The rich internal structure of molecules naturally lends themselves to extensive and exciting applications. In this paper, the radical $^{138}Ba^{19}F$, as a promising candidate for laser cooling and magneto-optical trapping, is discussed in detail. The highly diagonal Franck–Condon factors between the $X^2\Sigma^+_{1/2}$ and $A^2\Pi_{1/2}$ states are first confirmed with three different methods. Afterwards, with the effective Hamiltonian approach and irreducible tensor theory, the hyperfine structure of the $X^2\Sigma^+_{1/2}$ state is calculated accurately. A scheme for laser cooling is given clearly. Besides, the Zeeman effects of the upper ($A^2\Pi_{1/2}$) and lower ($X^2\Sigma^+_{1/2}$) levels are also studied, and their respective g factors are obtained under a weak magnetic field. Its large g factor of the upper state $A^2\Pi_{1/2}$ is advantageous for magneto-optical trapping. Finally, by studying Stark effect of BaF in the $X^2\Sigma^+_{1/2}$, we investigate the dependence of the internal effective electric field on the applied electric field. It is suggested that such a laser-cooled BaF is also a promising candidate for precision measurement of electron electric dipole moment.

**Keywords:** laser cooling, magneto-optical trapping, BaF radical

**PACS:** 37.10.Mn, 37.10.Pq, 32.10.Fn, 32.60.+i **DOI:** 10.1088/1674-1056/26/3/033702

## 1. Introduction

During the past three decades, studies of cold and ultracold atoms have been developed into a very mature field with tremendous achievements.[1,2] Now scientists are also eager to produce cold molecule samples, owing to their rich internal degrees of freedom, large electric dipole moments, chemical characteristics and so on, which atoms do not possess inherently. Inspired by their fascinating applications, such as the researches in the fields of cold reactive and inelastic collisions, precision measurements, quantum simulations, and so forth, cold molecules have become a very hot research point.[3–5] A variety of methods have been invented to create cold molecules. For instance, (ac) Stark decelerating[6–8] and Zeeman slowing[9] have been developed to the slow molecular beam to be a few meters per second with ∼mK temperature, while velocity filtering[10] and buffer gas cooling[11] have produced cold samples at tens of meters per second with ∼K temperature. Photo dissociation[12,13] and Feshbach resonance techniques[14,15] have also been successfully used to prepare ultra-cold molecular samples, but their lifetime is general short due to intermolecular collisions. Recently, the opto-electrical coolings of polyatomic molecules $CH_3F$ and $H_2CO$, as a new technical route to sub-mK temperatures, have been reported excitingly.[16]

As we all know, laser cooling and magneto-optical trapping are central to modern atomic physics, which can bridge the gap between cold and ultra-cold regime effectively. In spite of numerous difficulties, these techniques can be still extended to molecular systems promisingly. Following the proposal of Di Rosa,[17] if a certain molecule meets some criteria, it could be a promising candidate for laser cooling and magneto-optical trapping, like YO,[18] SrF,[19,20] CaF,[21,22] MgF,[23] and AlCl,[24] even SrOH.[25] Recently, CaF and YO radicals have been the laser cooled to near the capture velocity of magneto-optical trap (MOT), while SrF has been loaded into an MOT. More recently, optical cycling in SrOH and its transverse deflection have been demonstrated, which opens an unprecedented door to realize laser cooling of polyatomic molecules.

The reasons why we focus on the $^{138}Ba^{19}F$ radical, as a candidate for laser cooling and trapping, are explained as follows. Firstly, BaF is an important radical in astrophysical observations.[26] Many experimental studies about this radical provided some accurate and important spectroscopic data for 16 electronic states,[27–30] especially $X^2\Sigma^+_{1/2}$ and $A^2\Pi_{1/2}$. Secondly, it has highly diagonal Franck–Condon factors (FCFs) between $X^2\Sigma^+_{1/2}$ and $A^2\Pi_{1/2}$. Three laser beams can guarantee at least $10^4$ photon scatterings. Thirdly, it possesses a simple and special hyperfine structure (HFS) in $X^2\Sigma^+_{1/2}$ and a short lifetime $\tau \sim 56.0$ ns in the excited state $A^2\Pi_{1/2}$ (the sponta-

*Project supported by the National Natural Science Foundation of China (Grant Nos. 91536218, 11374100, 10904037, 10974055, 11034002, and 11274114), the National Key Basic Research and Development Program of China (Grant No. 2011CB921602), and the Natural Science Foundation of Shanghai Municipality, China (Grant No. 13ZR1412800).

†Corresponding author. E-mail: jpyin@phy.ecnu.edu.cn

© 2017 Chinese Physical Society and IOP Publishing Ltd 

neous decay rate $\Gamma \approx 2\pi \times 3$ MHz),[31] leading to a relatively large photon scattering rate. Fourthly, the Landé $g$ factor of BaF in $A^2\Pi_{1/2}$ is larger than that of YO, SrF, or CaF, which will strengthen its trapping force in MOT. Also the molecule BaF possesses a metastable state $A'^2\Delta$ between the $X^2\Sigma^+_{1/2}$ and $A^2\Pi_{1/2}$ states.[27] This makes it possible to prepare a narrow line MOT for BaF. Fifthly, it is a ground $^2\Sigma$ molecule with a free electron in its outermost orbital. When the electron whizzes through the heavy nucleus $^{138}$Ba, the possible P- (parity) and P,T- (time reversal) odd effects are enhanced relatively by three orders of magnitude than those in atoms, which have already been affirmed by many theoretical researches.[32–35] As a paramagnetic molecule with a large permanent electric dipole moment, it is easily polarized in small electric field. This can improve the statistical limit and suppress electric-field-induced systematic errors in electron electric dipole moment (eEDM) experiments,[36] and also provide the possibilities of exploring long-range dipole-dipole interaction and cold collisions controlled with an external electric field.[37]

Although BaF was previously suggested as being potentially amenable to Doppler cooling by *ab initio*,[38] some key problems still remain unsolved, such as accurate FCFs, HFS of the $X^2\Sigma^+_{1/2}$ state, the closure of rotational branching, the feasibility of magneto-optical trapping, and so on. Hence, it is necessary to precisely calculate the FCFs of BaF and the HFS of the $X^2\Sigma^+_{1/2}$ state, and to discuss the feasibility of laser cooling and magneto-optical trapping of BaF. We thus accomplish these researches and obtain some important new results.

Our article is organized as follows. In Section 2, a classical model for BaF is introduced for the following calculations. In Section 3, the highly diagonal FCFs of the main transitions are verified by three different methods, namely, a closed-form approximation, Morse approximation, and Rydberg–Klein–Rees (RKR) inversion. The probability of decay from the $A^2\Pi_{1/2}$ to $A'^2\Delta$ states is also evaluated. A scheme to form a quasi-closed cycle of vibrational transitions is given clearly. In Section 4, the HFS of lower $X^2\Sigma^+_{1/2}$ is studied using the effective Hamiltonian approach and irreducible tensor theory. Section 5 deals with Zeeman effects of upper ($A^2\Pi_{1/2}$) and lower ($X^2\Sigma^+_{1/2}$) levels, and gives their accurate $g$-factors. In Section 6, the Stark effect of BaF in $X^2\Sigma^+_{1/2}$ state is calculated. The molecular internal effective field as a function of the applied electric field is also studied. Some primary results and conclusions are made in Section 7.

## 2. A model for BaF

Our model of BaF is composed of a barium nucleus, a fluorine nucleus, and 65 electrons. According to the nonrelativistic Born–Oppenheimer (BO) approximation (electrons orbit around almost motionless nuclei adiabatically),[39] there are two freedom degrees for the relative motions of two nuclei, namely free rotation and stretching vibration. Their Hamiltonians are described by

$$\hat{H}_{\rm rot} = -\frac{\hbar^2}{2mr^2}\left[\frac{1}{\sin\theta}\frac{\partial}{\partial\theta}\left(\sin\theta\frac{\partial}{\partial\theta}\right)+\frac{1}{\sin^2\theta}\frac{\partial^2}{\partial\phi^2}\right], \quad (1)$$

$$\hat{H}_{\rm vib} = -\frac{\hbar^2}{2mr^2}\frac{\partial}{\partial r}\left(r^2\frac{\partial}{\partial r}\right), \quad (2)$$

where $\hbar$, $r$, and $m$ are the Planck constant, the internuclear distance, and the reduced mass of two nuclei, respectively. Generally, for linear molecules, the Euler angles $(\phi,\theta,\chi=0)$ define a relative orientation of the molecule-fixed coordinates with respect to the space-fixed coordinates, as shown in Fig. 1. Thus, we can also give the electronic Hamiltonian of BaF including the Coulomb repelling potential by

$$\hat{H}_{\rm el} = \sum_{i=1}^{65}\frac{P_i'^2}{2m_{\rm e}} + \frac{e^2}{4\pi\varepsilon_0}\left[\sum_{i<j}\frac{1}{r_{ij}} - \sum_{i=1}^{65}\left(\frac{Z_{\rm Ba}}{r_{{\rm Ba}i}}+\frac{Z_{\rm F}}{r_{{\rm F}i}}\right)+\frac{Z_{\rm Ba}Z_{\rm F}}{r}\right], \quad (3)$$

where $P'$ and $m_{\rm e}$ denote the momentum operator and the mass of an electron. The symbols $e$, $Z_{\rm Ba}e$, and $Z_{\rm F}e$ describe the electric charges of an electron, the barium nucleus, and the fluorine nucleus, respectively. $r_{ij}$ denotes the relative position of electrons $i$ and $j$. $r_{{\rm Ba}i}$ ($r_{{\rm F}i}$) presents the distance between electron $i$ and the barium nucleus (fluorine nucleus). $\varepsilon_0$ is the permittivity of vacuum.

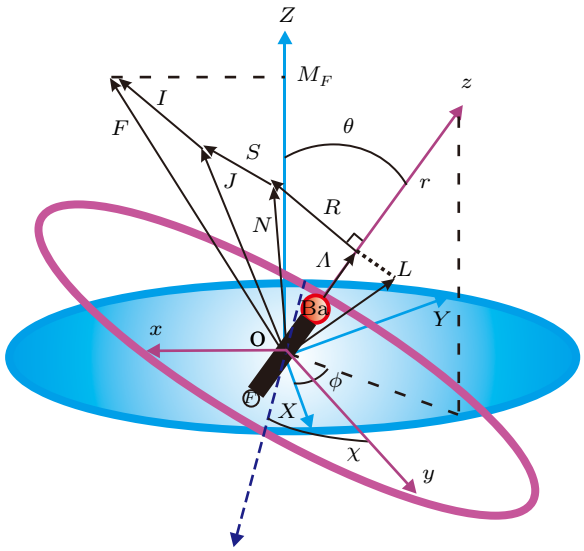



**Fig. 1.** (color online) The Euler angles $(\phi,\theta,\chi)$ define a relative orientation of the molecule-fixed coordinates $(x,y,z)$ with respect to the space-fixed coordinates $(X,Y,Z)$ for BaF depicted as a bar bell. The dotted blue line is the axis of nodes, which is the intersection of the $XY$ and $xy$ planes. The rotation–vibration motions of BaF in polar coordinates $(r,\phi,\theta)$ is discussed. Also shown is an angular momenta coupling diagram for Hund's case $(b_{\beta J})$ in the state $X^2\Sigma^+_{1/2}$.

In principle, an exact solution of the total Hamiltonian should give all information about BaF. However, this process is very cumbersome for this two-nuclei and super-multi-electron system. Since there are very accurate and abundant

spectroscopic data about this radical, the above BO approximation is an excellent choice for the following calculations. Here we will employ Eqs. (2) and (3) to determine the FCFs without considering nuclear rotations. Then the Hamiltonian of Eq. (1) will be replaced with an effective Hamiltonian, which will be used in the calculations of HFS, Zeeman shift, and electric field polarization.

## 3. The Franck–Condon factors between the $X^2\Sigma^+_{1/2}$ and $A^2\Pi_{1/2}$ states

The molecular FCFs are proportional to the square of the integral between the vibrational wave functions involved in optical transitions, and represent the vibrational branching ratios in molecular system. The Franck–Condon principle reminds us that $^{138}Ba^{19}F$ should be a good molecule for laser cooling because of the small difference ($\sim 0.022$ angstrom (Å) in equilibrium inter-nuclear distances between the states $X^2\Sigma^+_{1/2}$ and $A^2\Pi_{1/2}$.[40,41] Table 1 lists molecular parameters of BaF in the states $X^2\Sigma^+_{1/2}$and $A^2\Pi_{1/2}$ for the following calculations. We first employ a closed-form approximation to estimate FCFs based solely on $m$, $\omega_e$, and $r_e$.[42] The key point for calculating FCFs is the accuracy of the constructed potential energy curves. The Morse potential

$$U_{\text{Morse}}(r) = D_e\left[1 - e^{-a(r-r_e)}\right]^2 \tag{4}$$

provides a good approximation for the potential energy curve of the low vibrational levels, allowing an exact solution of Eqs. (2) and (3).[43] Note that $D_e$ is the bond energy in equilibrium position $r_e$, rather than $D_0$, the dissociation energy above the zero-point energy. The constant $a$ can be determined from a measurement of $\omega_e$ and $\omega_e\chi_e$. The RKR inversion uses WKB approximation to derive the classical turning point from the measured vibration–rotation constants, with which the whole potential energy curve can be then constructed point by point.[44] The RKR procedure is a most frequently used method and yields more exact results of FCFs.

**Table 1.** Molecular vibronic parameters for BaF in the $X^2\Sigma^+_{1/2}$ and $A^2\Pi_{1/2}$ states.

| Molecular parameters | $X^2\Sigma^+_{1/2}$ | $A^2\Pi_{1/2}$ | References |
|---|---|---|---|
| $T_e/\text{cm}^{-1}$ | 0 | 11646.9 | [27] |
| $\omega_e/\text{cm}^{-1}$ | 469.41 | 435.5 | [27] |
| $\omega_e\chi_e/\text{cm}^{-1}$ | 1.836 | 1.68 | [27] |
| $r_e$/Å | 2.161 | 2.183 | [40], [41] |
| $\tau$/ns | – | 56.0 | [31] |

We first discuss the electronic decay paths. The transition frequency between $A$ and $A'$ is smaller than that for the $A$–$X$ transition: $\omega_{AX}/\omega_{AA'} \approx 12$.[27] The $A$–$A'$ transition dipole moment is much smaller than that of the $A$–$X$ transition: $d_{AX}/d_{AA'} \approx 68$.[38] Since the decay rate $\gamma \propto d^2\omega^3$, we can estimate that $\gamma_{AA'}/\gamma_{AX} \approx 10^{-6}$. As such, the unwanted $A$–$A'$ leak is unlikely to limit the laser cooling process significantly. Hence, we can choose the transition $A^2\Pi_{1/2} \leftarrow X^2\Sigma^+_{1/2}$ as a cooling channel.

For the $A$–$X$ transition, the results we calculated about FCFs by three methods are in good agreement with each other. Recently, Chen and others[45] also reported similar results about FCFs, as shown in Table 2. This means that our calculations are accurate and reliable. Since the transitional wavelengths reported in Ref. [38] are significantly different from the experimental values,[27] the potential curve calculated by *ab initio* seems to be inaccurate. The sum of $f_{00}$, $f_{01}$, and $f_{02}$ is very close to unity, greater than 0.9999, so with three lasers, a BaF molecule can scatter about $10^4$ photons before decaying into the higher vibrational dark states ($v \geq 3$) in $X^2\Sigma^+_{1/2}$. This is sufficient to laser cooling BaF beam from cryogenic buffer-gas source. This Doppler cooling scheme has a main cooling transition $\lambda_{00} = 859.8$ nm from $X^2\Sigma^+_{1/2}$ $(v = 0)$ to $A^2\Pi_{1/2}$ $(v' = 0)$ because of its favorable FCFs ($f_{00} = 0.9371$), as shown in Fig. 2. Then the vibrational leakages can be addressed by repumping the $X^2\Sigma^+_{1/2}$ $(v = 1)$ directly to the $A^2\Pi_{1/2}$ $(v' = 1)$, also the $(v = 2)$ to the $(v' = 1)$. The choice of repumping $X^2\Sigma^+_{1/2}$ $(v = 1)$ through the same excited state $A^2\Pi_{1/2}$ $(v' = 0)$ used on the main cycling transition is a matter of convenience,[18,20,22] but there are some deleterious effects in this case. According to the maximum scattering equation $\max(R_{sc}) = \Gamma N_e/(N_g + N_e)$,[46] this $\Lambda$-system structure doubles the number of ground states $N_g$ coupled into the optical cycle, reducing the maximum scattering rate to $\Gamma/7$ compared with $\Gamma/4$ in ours (for each vibrational state, there are twelve hyperfine levels of $X$ and four hyperfine levels of $A$ participating in cooling process). So such an alternate repumping pathway would significantly reduce the required distance for slowing. Thus the vibrational quasi-closed transitions have been completed in principle. Fortunately, these transitional wavelengths can be offered by semiconductor lasers.

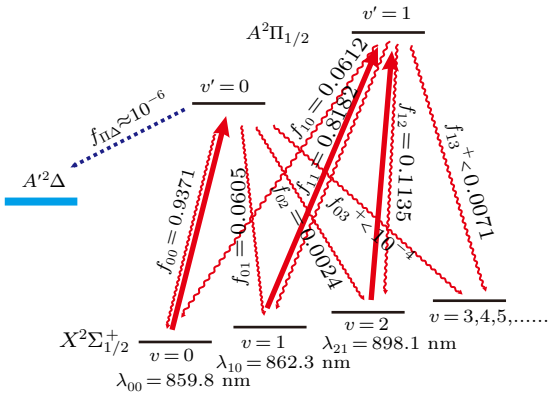



**Fig. 2.** (color online) The proposed scheme to create quasi-closed transitions for laser cooling of BaF. Solid black lines indicate the relevant electronic and vibrational structures in BaF. Red upward lines denote laser-driven transitions at the wavelengths $\lambda_{vv'}$. Wavy lines represent spontaneous decays from the $A^2\Pi_{1/2}$ state with FCFs $f_{v'v}$. The leakages from $A^2\Pi_{1/2}$ to $A'^2\Delta$ (cyan) is described by the dotted blue line.

**Table 2.** Our calculated FCFs $f_{v'v}$ of BaF in contrast with other results. These transitions happen from the $A^2\Pi_{1/2}$ ($v'$) to $X^2\Sigma^+_{1/2}$ ($v$) states.

| Methods | $f_{00}$ | $f_{01}$ | $f_{02}$ | $f_{03}$ | $f_{10}$ | $f_{11}$ |
|---|---|---|---|---|---|---|
| A closed-form potential | 0.9473 | 0.0513 | 0.0014 | 0.0000 | 0.0513 | 0.8475 |
| Morse potential | 0.9470 | 0.0514 | 0.0016 | 0.0000 | 0.0522 | 0.8450 |
| RKR potential | 0.9371 | 0.0605 | 0.0024 | 0.0000 | 0.0612 | 0.8182 |
| Ref. [38] | 0.9810 | 0.0189 | 0.000396 | 0.0000 | 0.0192 | 0.9400 |
| Ref. [45] | 0.9508 | 0.0476 | 0.0015 | 0.000027 | 0.0483 | 0.8539 |

## 4. Hyperfine structure of the $^{138}$Ba$^{19}$F radical

In this section, we will take into account rotational HFS ladders in the ground states $X^2\Sigma^+_{1/2}$, which play important roles in eliminating dark states and implementing nearly closed electric dipole transitions. In the eEDM experiment, these ladders can be utilized to prepare a Ramsey interferometer to acquire phase shifts.[47,48] Unlike vibrational states, the transitions in the rotational HFS still follow strict angular momentum and parity selection rules, fortunately.

We begin by introducing the effective Hamiltonian,[49] which describes all kinds of intercouplings of degrees of freedom in a molecular system. The effective Hamiltonian operates only within the levels (fine and hyperfine) of a given vibrational state of the particular electronic state of interest, but it can reproduce the eigenenergy of the full Hamiltonian, which is more complicated than the sum of Eqs. (1)–(3). Actually, for a typical heavy diatomic molecule, the effective Hamiltonian can be described by

$$\begin{aligned}\hat{H}_{\rm eff} &= \hat{T}_0+\hat{H}_{\rm SO}+\hat{H}_{\rm SS}+\hat{H}_{\rm SR}+\hat{H}_{\rm Rot}+\hat{H}_{\rm CD}+\hat{H}_{\rm LD}\\ &\quad+\hat{H}_{\rm M}+\hat{H}_{\rm Q}+\hat{H}_{\rm Stark}+\hat{H}_{\rm Zeeman}+\hat{H}_{\rm relativity},\end{aligned}\tag{5}$$

where $\hat{T}_0$, $\hat{H}_{\rm SO}$, $\hat{H}_{\rm SS}$, $\hat{H}_{\rm SR}$, $\hat{H}_{\rm Rot}$, $\hat{H}_{\rm CD}$, $\hat{H}_{\rm LD}$, $\hat{H}_{\rm M}$, and $\hat{H}_{\rm Q}$ represent the vibronic energy, the electronic spin–orbit interaction, the electronic spin–spin interaction, the electronic spin–nuclear rotational interaction, the nuclear rigid rotation energy, the centrifugal distortion energy, Λ-doubling splitting, the magnetic hyperfine interactions, and the nuclear electric quadruple interaction, respectively. $\hat{H}_{\rm Stark}$ and $\hat{H}_{\rm Zeeman}$ are the Hamiltonians of external field effects in the experiment. Besides, $^{138}$Ba$^{19}$F contains a highly electronegative element F and a heavy element Ba with two valence electrons, in which an unpaired electron will feel strong relativistic effects.[32] Hence, the last term denotes the relativistic effect in this radical, often including the parity non-conservation (PNC) relevant operators. In this section, we discuss the field-free HFS only, and the last three terms will be treated in the following sections.

The molecule $^{138}$Ba$^{19}$F has the electronic ground state $X^2\Sigma^+_{1/2}$, which is near the Hund's case ($b_{\beta J}$) limit[49,50] with the approximately good intermediate quantum number $J$ resulting from coupling the rotational angular momentum $N$ with the electron spin angular momentum $S$, as depicted in Fig. 1. The electron orbital angular momentum is labeled as $L$. Its projection onto the internuclear $z$ axis is described by $\Lambda$ while the end-over-end rotational angular momentum of the nuclei and total angular momentum are labeled as $R$ and $F$ respectively. $\Lambda$ is coupled with $R$ to form $N$; finally $J$ is coupled with $I$ to form $F$, which corresponds to the basis set $|v\Lambda N(S)J(I)FM_F\rangle$, therein $v$ denotes the vibrational quantum number and $M_F$ is the projective component of $F$ in a space-fixed $Z$ axis. Here BaF has an unpaired electron with spin $S=1/2$ and the orbital projection $\Lambda=0$, so we neglect spin–spin coupling $\hat{H}_{\rm SS}$ and the terms about the electronic orbit, like $\hat{H}_{\rm SO}$, $\hat{H}_{\rm LD}$. For a nucleus with spin $I$, the $2^l$-pole electrostatic interaction is zero if $l$ is greater than $2I$.[49] From parity considerations, $l$ can only take an even integer. For this isotope, $^{138}$Ba$^{19}$F, the nuclear spins of the barium nucleus and the fluorine nucleus are $I_{\rm Ba}=0$ and $I_{\rm F}=1/2$. For the electric quadruple interaction, $l=2$ is larger than $2I_{\rm F}=1$, so we take no account of this interaction. Meanwhile, for convenience, we take $\hat{T}_0$ equal to zero in the detailed calculation. The spherical tensor operators are very useful in dealing with angular momenta problems, especially when combined with the Wigner–Eckart theorem.[51] Matrix elements of operators can be reduced to the product of two parts. One part expresses the geometry, symmetry, and section rules of system, and the other part contains the dynamics. Thus for this radical, the effective Hamiltonian of Frosch and Foley can be written as[52]

$$\begin{aligned}\hat{H}_{\rm eff} &= B_v\hat{N}^2-D_v\hat{N}^4+\gamma_v T^1(\hat{S})\cdot T^1(\hat{N})+b_{{\rm F}v}T^1(\hat{I})\cdot T^1(\hat{S})\\ &\quad-\sqrt{10}g_{\rm S}\mu_{\rm B}g_{\rm N}\mu_{\rm N}(\mu_0/4\pi)T^1(\hat{S},C^2)\cdot T^1(\hat{I})\\ &\quad+C_{v{\rm N}}T^1(\hat{I})\cdot T^1(\hat{N}),\end{aligned}\tag{6}$$

where $B_v$, $D_v$, $\gamma_v$, and $b_{{\rm F}v}$ represent the molecular rotational constant, the centrifugal distortion constant, the spin–rotational coupling constant, and the Fermi contact interaction constant, respectively, as shown in Table 3. The fifth term specifies the dipole–dipole interaction between the electron spin and nuclear spin, therein $g_{\rm S}$, $\mu_{\rm B}$, $g_{\rm N}$, $\mu_{\rm N}$, and $\mu_0$ are free electron g factor, Bohr magneton, nuclear $g$ factor, nuclear Bohr magneton, and magnetic constants, respectively. The last term describes the nuclear spin–rotational coupling, which is often neglected. Based on the above basis set and the effective Hamiltonian of Eq. (6), combined with the spherical tensor algebra, we can obtain the five matrix representations in Appendix B. Then we can obtain the field-free eigenvalues and eigenvectors for the $X^2\Sigma^+_{1/2}$ state by numerical diagonalization of the effective Hamiltonian matrix representations. To check the accuracy of the results we calculated, we compare them with observed rotational microwave spectra[53] in Table 4. The differences between them are less than the one-sixth of line width of the upper state $A^2\Pi_{1/2}$, $\Gamma\approx(2\pi\times3\ {\rm MHz})$,[31] which

nicely meet the requirement of laser cooling and trapping experiments.

**Table 3.** Rotational and hyperfine structure parameters and electric dipole moment for the $X^2\Sigma^+_{1/2}$ ($v=0$) state of $^{138}$Ba$^{19}$F.[50]

| Molecular parameters | $X^2\Sigma^+_{1/2}$ |
|---|---|
| $B_0/\mathrm{cm}^{-1}$ | 0.21594802 |
| $D_0/\mathrm{cm}^{-1}$ | $1.85\times10^{-7}$ |
| $\gamma_0/\mathrm{cm}^{-1}$ | $2.6993\times10^{-3}$ |
| $b_{\mathrm{F}0}/\mathrm{cm}^{-1}$ | $2.209862\times10^{-3}$ |
| $c_0/\mathrm{cm}^{-1}$ | $2.74323\times10^{-4}$ |
| $\mu_e$/Debye | 3.1702 |

**Table 4.** Hyperfine microwave transition frequencies for BaF in the $v=0$, $X^2\Sigma^+_{1/2}$ ground state.

| $N\to N'$ | $J\to J'$ | $F\to F'$ | $\nu_{\mathrm{obs}}$/MHz[53] | $\nu_{\mathrm{calc}}$/MHz | $\nu_{\mathrm{obs}}-\nu_{\mathrm{calc}}$/MHz |
|---|---|---|---|---|---|
| $0\to1$ | $1/2\to3/2$ | $0\to1$ | 13020.286 | 13020.787 | −0.501 |
| | | $1\to2$ | 12988.110 | 12988.082 | 0.028 |
| $1\to2$ | $1/2\to3/2$ | $0\to1$ | 25865.572 | 25856.067 | |
| | | $1\to2$ | 25854.434 | 25854.568 | −0.134 |
| $1\to2$ | $3/2\to5/2$ | $1\to2$ | 25936.873 | 25936.747 | 0.126 |
| | | $2\to3$ | 25936.006 | 25936.002 | 0.004 |

As plotted in Fig. 3, due to the interaction of $S=1/2$ and $I_{\mathrm{F}}=1/2$, each rotational state $N$ with the parity $(-1)^N$ in $X^2\Sigma^+_{1/2}$ splits into four hyperfine sublevels except the state of $N=0$. For the upper state $A^2\Pi_{1/2}$, it is best described by Hund's case ($a_{\beta J}$).[50] Each rotational $J$ state has a pair of $\Lambda$-doubling splitting with opposite parities, and levels with parity $(-1)^{J-1/2}$ or $(-1)^{J+1/2}$ are defined as $e$ or $f$. One can choose a transition $N=1$, $X^2\Sigma^+_{1/2}\to J'=1/2$ ($e$), $A^2\Pi_{1/2}$ to avoid rotational branchings within each vibrational manifold. On the basis of parity and angular momentum selection rules $\Delta J=0,\ \pm1$ and $\Delta F=0,\ \pm1$ for electric dipole transitions. This scheme can keep the molecules always in the rotational optical cycle. The complex internal degrees of freedom of molecules render the use of a Zeeman slower difficult.

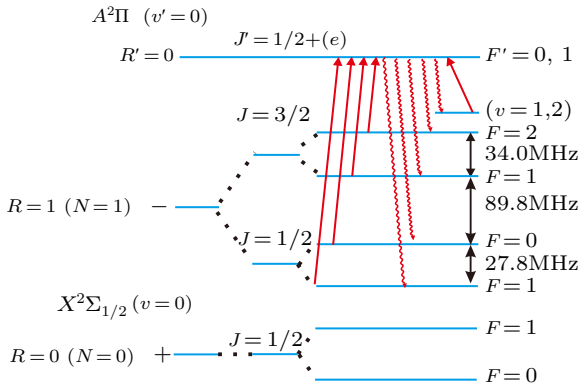



**Fig. 3.** (color online) The relevant rotational energy-level structure for laser cooling BaF. According to selection rules of the electric dipole transition, a $J'=1/2$ ($e$), ($A^2\Pi_{1/2}$) $\leftarrow N=1$, ($X^2\Sigma^+_{1/2}$) cycle can be chosen to avoid rotational branchings. The main cooling laser and other repumping lasers should be modulated into four components to cover HFS in $X^2\Sigma^+_{1/2}$. The calculated HFS intervals are also shown.

A "white-light" approach can be utilized to cover the hyperfine splitting and compensate the decreasing Doppler shifts, analogous to the method for CaF.[21] An alternative approach which would maintain fast photon-scattering rate is synchronously chirped cooling, which was successfully implemented with YO and CaF.[18,22] It is clear that those approaches can be used to prepare a BaF MOT efficiently.

## 5. Zeeman effects for MOT

In this section, a term associated with magnetic field will be added to Eq. (6) to study Zeeman effects of BaF because they play important roles in MOT, where the magnetic field gradient generates a space dependence of transitions, leading to a restoring force from radiation pressure. For a molecular system, the Zeeman interactions can be written as

$$\begin{aligned}\hat{H}_{\mathrm{Zeeman}} &= -T^1(\hat{\mu}_{\mathrm{M}})T^1_{p=0}(\hat{B})\\ &= g_{\mathrm{S}}\mu_{\mathrm{B}}T^1(\hat{S})T^1_{p=0}(\hat{B})+g_{\mathrm{L}}\mu_{\mathrm{B}}T^1(\hat{L})T^1_{p=0}(\hat{B})\\ &\quad -g_r\mu_{\mathrm{B}}T^1(\hat{J}-\hat{S}-\hat{L})T^1_{p=0}(\hat{B})\\ &\quad -g_{\mathrm{N}}\mu_{\mathrm{N}}T^1(\hat{I})T^1_{p=0}(\hat{B}),\end{aligned}\tag{7}$$

which contains, in order, the electronic spin Zeeman effect, the electronic orbital Zeeman effect, the nuclear rotational Zeeman effect, and the nuclear spin Zeeman effect. The free electron g factor and electron orbital g factor are approximately equal to 2.002 and 1, respectively. Because the projection $\Lambda$ of $L$ onto the $z$ axis is equal to zero and the molecule will precess around the external magnetic field, which is along the $Z$ direction ($p=0$), the second term about orbital Zeeman effect vanishes. Since $g_r$ is generally smaller than $g_{\mathrm{s}}$ by four orders of magnitude and $\mu_{\mathrm{B}}/\mu_{\mathrm{N}}\approx1836$, the first term makes a major contribution to the Zeeman effect. Here the subscripts $p$ and $q$ specify the components of tensors of rank 1 in the space- and molecule-fixed coordinate systems, respectively.[49] We can derive matrix elements of Zeeman Hamiltonians, as shown in Appendix A.

Figure 4 shows the magnetic tuning of hyperfine levels of $N=1$ in $X^2\Sigma^+_{1/2}$ for BaF. We can find that under weak magnetic field, the Landé $g$ factors of four sublevels do not share the same sign. The $|J=3/2,F=1\rangle$ and $|J=3/2,F=2\rangle$ states have positive magnetic $g$ factors, while the $g$ factor of $|J=1/2,F=1\rangle$ is a negative value. Unlike atoms, there are complex interactions of degrees of freedom in molecules, so the ideal coupling model does not exist actually, resulting in different magnetic $g$-factors. Table 5 gives the comparison of effective $g$-factors in ideal and actual cases. From the perspective of the eigenvector, it can be found that the mixing of different $J$ states makes the $g$-factors of $|J=3/2,F=1\rangle$ and $|J=1/2,F=1\rangle$ change, but the sum of both still equals 0.5.

**Table 5.** The $g$ factors of the $X^2\Sigma^+_{1/2}$ $(N=1)$ manifolds $|J,F\rangle$ without and with considering the mixing of $J$. These values are reliable only for small magnetic fields.

| $g$ factor | $\|3/2,2\rangle$ | $\|3/2,1\rangle$ | $\|1/2,0\rangle$ | $\|1/2,1\rangle$ |
|---|---|---|---|---|
| Ideal $g$ | 0.50 | 0.83 | 0.00 | −0.33 |
| Actual $g$ | 0.50 | 1.00 | 0.00 | −0.50 |

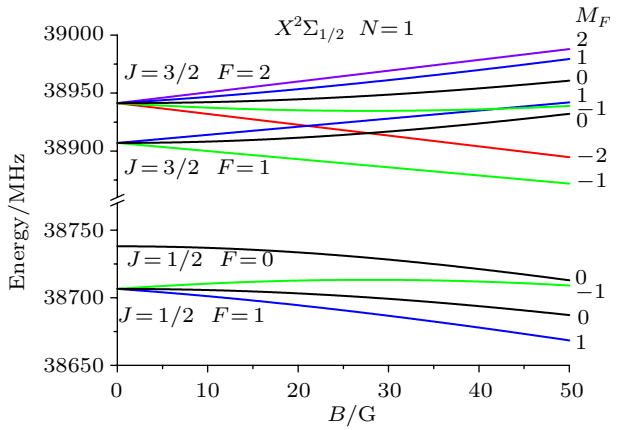



**Fig. 4.** (color online) Energy levels of the $X^2\Sigma^+_{1/2}$ $(v=0,\ N=1)$ state versus the magnetic field. The relevant levels are labeled by their $M_F$ values at zero field with $M_F=2$ (violet line), $M_F=1$ (blue line), $M_F=0$ (black line), $M_F=-1$ (green line), and $M_F=-2$ (red line).

As for the rotational state $J'=1/2\ (e)$ of the $A^2\Pi_{1/2}$ state, its g factor is typically small in Hund's case $(a_{\beta J})$ limit because the magnetic moments associated with the electron orbital and spin angular momentum are antiparallel on the internuclear axis, that is, $g_{\rm L}\Lambda+g_{\rm s}\Sigma\approx 0$. $\Sigma$ is the projection component of the electronic spin angular momentum onto the internuclear $z$ axis. In reality, an $A^2\Pi_{1/2}$ is usually mixed by rotational and spin–orbit interaction with nearby $^2\Sigma^+_{1/2}$. The most important terms to the effective $g$ factors about this mixing are the two parity-dependent coefficients $g_{l'}$ and $g_r^{\rm e'}$. An estimate for them is obtainable from the Curl relationship:[54]

$$g_{l'}=p_\Lambda/(2B)g_r^{\rm e'}=-q_\Lambda/B, \tag{8}$$

where $p_\Lambda$ and $q_\Lambda$ are the $\Lambda$-doubling parameters in the $A^2\Pi$ manifold. The parity-dependent anisotropic $g$-factors for $A^2\Pi_{1/2}$ can be approximated by

$$g_\pm=\pm\frac{1}{3}\left(g_{l'}-g_r^{\rm e'}\right). \tag{9}$$

Table 6 gives the effective $g$-factor of the $J'=1/2\ (e)$ of several relevant radicals in $A^2\Pi_{1/2}$. For most atomic MOTs, the main cooling cycle is a transition between lower and upper levels with angular momenta $F_l$ and $F_u=F_l+1$. This is the type I of MOT.[19] Since there are no dark Zeeman levels in this case, atoms feel a strong trapping force, and are always in the MOT. However, the case is different from the present molecular MOT. To implement the closure of rotational ladders, we have to choose the transitions $J=1/2(-)$ and $J=3/2(-)$, $X^2\Sigma^+_{1/2}\rightarrow J'=1/2\ (e)$, $A^2\Pi_{1/2}$, then $\rm F_\Pi\leq F_\Sigma$ (type II).[19] According to Ref. [55], the magnitude of upper-$g$ factor determines the trapping and cooling force of MOT since their lower-$g$ factors have small differences. As shown in Table 6, the $A^2\Pi_{1/2}$ $g$-factor of BaF is about twice that of SrF, even larger than that of CaF by one order of magnitude. We would expect its better performance in DC or RF MOT because the restoring force is nearly proportional to the upper-$g$ factor.[55,59] To prepare MOT for BaF, more scattering photons should be required in further cooling step. Some dark states must be remixed into the optical cycling with more repumping lasers or microwaves, like YO experiment.[18]

**Table 6.** The $g$-factor of the $J'=1/2\ (e)$ of a few relevant molecules in $A^2\Pi_{1/2}$.

| Molecules | $B$/cm$^{-1}$ | $p_\Lambda+2q_\Lambda$/cm$^{-1}$ | References | $g_{\rm e}$ |
|---|---|---|---|---|
| CaF | 0.34748 | −0.0439 | [56] | −0.0211 |
| SrF | 0.25135 | −0.13291 | [57] | −0.088 |
| YO | 0.385785 | −0.15061 | [58] | −0.065 |
| BaF | 0.21174 | −0.25755 | [50] | −0.2027 |

## 6. Electric polarizability for the eEDM measurement

Heavy atoms and molecules with unpaired spins provide a suitable environment for eEDM measurement.[60] For atomic systems, the external electric field linearly polarizes the electron cloud of atoms, so we can employ the enhancement factor $R$ to describe this relativistic effect. However, in polar molecules, the wave functions with opposite parities are naturally mixed, resulting in a strong polarization along the internuclear axis. Certainly, there are also other P- and P, T–odd interactions in this system. The effective Hamiltonians for BaF are described by[32]

$$H_{\rm PNC}=W_{\rm A}k_{\rm A}\boldsymbol{n}\times\boldsymbol{IS}+(W_{\rm S}k_{\rm S}+W_{\rm d}d_{\rm e})\,\boldsymbol{Sn}, \tag{10}$$

where $\boldsymbol{n}$ is an unit vector along the molecular bond. The first term refers to the interaction of the anapole moment of the nucleus $k_{\rm A}$ with $S$, which will be neglected because this isotope $^{138}$Ba has no nuclear spin. The last term describes the scalar electron–nucleus interaction $W_{\rm S}k_{\rm S}$[34] and the interaction of eEDM $d_{\rm e}$ with the effective electric field constant $W_{\rm d}$. Thereby the eEDM is not only the possible source of a phase shift proportional to $\boldsymbol{S}\cdot\boldsymbol{n}$. However, following the usual convention, the result is still interpreted entirely in terms of an eEDM. However, the PNC parameter $W_{\rm d}$ cannot be measured directly. Its magnitude can be calculated by relativistic electronic-structure methods, about $-0.4\times10^{25}$ Hz/e·cm.[32]

However, molecules are free to rotate in the three-dimensional space, so $W_{\rm d}$ averages to zero, that is, $\langle\boldsymbol{S}\cdot\boldsymbol{n}\rangle=0$, an external electric field is required to orientate molecular axis. This interaction can be written as

$$\hat{H}_{\rm Stark}=-T^1_{q=0}\left(\hat{\mu}_{\rm e}\right)T^1_{p=0}\left(\hat{E}\right), \tag{11}$$

where $\mu_e$ is the permanent electric dipole moment of BaF in $X^2\Sigma^+_{1/2}$. The electric field is also applied along the $Z$ direction. Its matrix representation is described in Appendix A. Because the electric dipolar moment has the property of T-symmetry, the states $|F, M_F\rangle\rangle$ and $|F, -M_F\rangle$ are always exactly degenerate under the whole electric field. Thus we can get the variation of $W_d$ with the external electric E for BaF in the rovibrational ground levels $N = 0$, $F = 1$, $M_F = 1$, which are the quantum interference states in the eEDM experiment. For an applied electric field at 10 kV/cm in the usual experiments,[47] the effective field constant experienced by the valence electron in BaF is about $-9.08$ GV/cm, as depicted in Fig. 5. With such a strong internal electric field, maybe this radical is also a promising candidate for precision measurement of eEDM after being laser cooled.

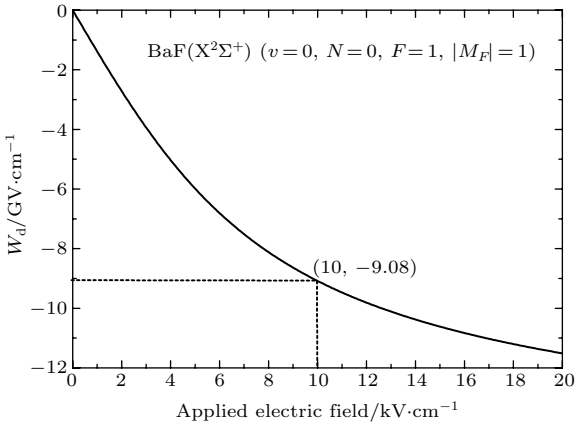



**Fig. 5.** The PNC constant $W_d$ for BaF as a function of the applied electric field. The dashed line shows the available operating field 10 kV/cm in the eEDM experiment. The negative sign indicates this effective field points in the opposite direction to the molecular EDM.

## 7. Conclusions

In this paper, the Franck–Condon factors between the $X^2\Sigma^+_{1/2}$ and $A^2\Pi_{1/2}$ states have been calculated in the framework of Born–Oppenheimer approximation. Results by three different methods agree well with each other. With the effective Hamiltonian approach, we have studied the HFS of $X^2\Sigma^+_{1/2}$ and Zeeman effects of $X^2\Sigma^+_{1/2}$ and $A^2\Pi_{1/2}$. It is found that the g factor of the upper level is larger than that of SrF, CaF, or YO. Our studies indicate that the $^{138}Ba^{19}F$ radical is a promising candidate for laser cooling and magneto-optical trapping. Finally, Stark effect of BaF in $X^2\Sigma^+_{1/2}$ is investigated and the dependence of the effective electric field in BaF on the applied external electric field for the eEDM experiment is obtained. Once the BaF molecules are laser cooled to near the capture velocity of a MOT, their valuable applications can be found in ultra-cold physics and precision measurement.

## Appendix A: Spherical tensor algebra

Supposing that $\hat{A}$ and $\hat{B}$ are arbitrary vector operators with their space-fixed components $(\hat{A}_X, \hat{A}_Y, \hat{A}_Z)$ and $(\hat{B}_X, \hat{B}_Y, \hat{B}_Z)$ and molecule-fixed components $(\hat{A}_x, \hat{A}_y, \hat{A}_z)$ and $(\hat{B}_x, \hat{B}_y, \hat{B}_z)$, the rank-1 irreducible spherical tensor operator $T^1(\hat{A})$ is given by

$$T^1_{p=1}(\hat{A}) = -\frac{1}{\sqrt{2}}(\hat{A}_X + \mathrm{i}\hat{A}_Y), \quad T^1_{p=0}(\hat{A}) = \hat{A}_Z,$$
$$T^1_{p=-1}(\hat{A}) = \frac{1}{\sqrt{2}}(\hat{A}_X - \mathrm{i}\hat{A}_Y). \tag{A1}$$

The scalar product of two rank-1 spherical tensor becomes

$$T^1(\hat{A}) \cdot T^1(\hat{B}) = \sum_{p=0,\pm1} (-1)^p T^1_p(\hat{A})\, T^1_{-p}(\hat{B}). \tag{A2}$$

The transformation of a rank-1 spherical tensor from space ($p$) to molecular ($q$) axes via the matrix elements of the Wigner $D$-matrix, $D^{(1)}_{p,q}(\phi,\theta,\chi)$ or $D^{(1)}_{p,q}(\omega)$, and vice versa, are given by

$$T^1_q(\hat{A}) = \sum_{p=0,\pm1} D^{(1)}_{p,q}(\omega) T^1_p(\hat{A}),$$
$$T^1_p(\hat{A}) = \sum_{q=0,\pm1} D^{(1)*}_{p,q}(\omega) T^1_q(\hat{A}). \tag{A3}$$

The Wigner–Eckart theorem gives the matrix elements of the spherical tensor operators,

$$\langle j', m'_j | T^1_p(\hat{A}) | j, m_j \rangle = \delta_{j'j}(-1)^{j'-m'_j} \begin{pmatrix} j' & l & j \\ -m'_j & p & m_j \end{pmatrix} \langle j' || T^1(\hat{A}) || j \rangle, \tag{A4}$$

where $T^1_p(\hat{A})$ operates on angular momentum $\hat{j}$ and $\hat{j}$'s projective value onto the $Z$ axis is described by $m_j$. $\langle j' || T^1(\hat{A}) || j \rangle$, called reduced matrix element, is defined as $\langle j' || T^1(\hat{j}) || j \rangle = \delta_{j'j}\sqrt{j(j+1)(2j+1)}$. The Kronecker delta function $\delta_{i'i}$ is defined as having the properties that $\delta_{i'i} = 0$ for $i' \neq i$ and $\delta_{i'i} = 1$ for $i' = i$. Hence, the matrix element of rotational matrix is given by

$$\langle j', \Omega'_j, m'_j | D^{(1)*}_{p,q}(\omega) | j, \Omega_j, m_j \rangle = \delta_{j'j}(-1)^{j'-m'_j} \begin{pmatrix} j' & 1 & j \\ -m'_j & p & m_j \end{pmatrix} \langle j', \Omega'_j | D^{(1)*}_q(\omega) | j, \Omega \rangle. \tag{A5}$$

Here the reduced matrix element is given by

$$\langle j', \Omega'_j | D^{(1)*}_q(\omega) | j, \Omega \rangle = (-1)^{j'-\Omega'_j} \begin{pmatrix} j' & 1 & j \\ -\Omega'_j & q & \Omega_j \end{pmatrix} \sqrt{(2j'+1)(2j+1)}, \tag{A6}$$

where $\Omega$ is the projective quantum number of $\hat{j}$ along the $z$ direction. For matrix element of a scalar product, we can obtain

$$\langle j'_1, j'_2, j'_{12}, m'_{j_{12}} | T^1(\hat{A}_1) \cdot T^1(\hat{B}_2) | j_1, j_2, j_{12}, m_{j_{12}} \rangle = \delta_{j'_{12} j_{12}} \delta_{m'_{j_{12}} m_{j_{12}}} (-1)^{j_1 + j'_{12} + j'_2} \begin{Bmatrix} j_2 & j_1 & j'_{12} \\ j'_1 & j'_2 & k \end{Bmatrix} \times \langle j'_1 || T^1(\hat{A}_1) || j_1 \rangle \langle j'_2 || T^1(\hat{B}_2) || j_2 \rangle, \tag{A7}$$

where $T^1\left(\hat{A}_1\right)$ and $T^1\left(\hat{B}_2\right)$ operate on angular momentum $\hat{j}_1$ and $\hat{j}_2$ respectively. For a single operator in a coupled scheme, we then obtain

$$\begin{aligned}&\left\langle j_1', j_2', j_{12}'\right|\left|T^1\left(\hat{A}_1\right)\right|\left|j_1, j_2, j_{12}\right\rangle\\&=\delta_{j_2' j_2}(-1)^{j_{12}+j_1'+j_2'+1}\sqrt{\left(2j_{12}'+1\right)\left(2j_{12}+1\right)}\\&\quad\times\left\{\begin{array}{ccc} j_1 & j_{12} & j_2' \\ j_{12}' & j_1' & 1\end{array}\right\}\left\langle j_1'\right|\left|T^1\left(\hat{A}_1\right)\right|\left|j_1\right\rangle.\end{aligned}\tag{A8}$$

Similarly, for the matrix element of $T^1\left(\hat{B}_2\right)$, we have

$$\begin{aligned}&\left\langle j_1', j_2', j_{12}'\right|\left|T^1\left(\hat{B}_2\right)\right|\left|j_1, j_2, j_{12}\right\rangle\\&=\delta_{j_1' j_1}(-1)^{j_{12}'+j_1'+j_2+1}\sqrt{\left(2j_{12}'+1\right)\left(2j_{12}+1\right)}\\&\quad\times\left\{\begin{array}{ccc} j_2 & j_{12} & j_1' \\ j_{12}' & j_2' & 1\end{array}\right\}\left\langle j_2'\right|\left|T^1\left(\hat{B}_2\right)\right|\left|j_2\right\rangle.\end{aligned}\tag{A9}$$

## Appendix B: Matrix representations for the effective Hamiltonian

For this BaF radical, we have chosen a Hund's case ($b_{\beta j}$) basis $|v\Lambda N(S)J(I)FM_F\rangle$ to obtain matrix representations for the effective Hamiltonian, as follows:

(i) Molecular rotation

$$\begin{aligned}&\left\langle v'\Lambda'N'(S)J'(I)F'M_F'\right|B_v\hat{N}^2-D_v\hat{N}^4\left|v\Lambda N(S)J(I)FM_F\right\rangle\\&=\delta_{v'v}\delta_{\Lambda'\Lambda}\delta_{N'N}\delta_{J'J}\delta_{F'F}\delta_{M_F'M_F}N(N+1)\\&\quad\times\left[B_v-D_vN(N+1)\right].\end{aligned}\tag{B1}$$

(ii) Spin–molecular rotation coupling

$$\begin{aligned}&\left\langle v'\Lambda'N'(S)J'(I)F'M_F'\right|\gamma_vT^1\left(\hat{S}\right)\cdot T^1\left(\hat{N}\right)\left|v\Lambda N(S)J(I)FM_F\right\rangle\\&=\delta_{v'v}\delta_{\Lambda'\Lambda}\delta_{N'N}\delta_{J'J}\delta_{F'F}\delta_{M_F'M_F}\gamma_v(-1)^{N+J+S}\\&\quad\times\left[S(S+1)(2S+1)\right]^{1/2}\left[N(N+1)(2N+1)\right]^{1/2}\\&\quad\times\left\{\begin{array}{ccc} S & N & J \\ N & S & 1\end{array}\right\}.\end{aligned}\tag{B2}$$

(iii) Magnetic hyperfine interaction (I)

$$\begin{aligned}&\left\langle v'\Lambda'N'(S)J'(I)F'M_F'\right|b_{Fv}T^1\left(\hat{I}\right)\cdot T^1\left(\hat{S}\right)\left|v\Lambda N(S)J(I)FM_F\right\rangle\\&=\delta_{v'v}\delta_{\Lambda'\Lambda}\delta_{N'N}\delta_{F'F}\delta_{M_F'M_F}b_{Fv}(-1)^{J'+F+I+J+N+1+S}\\&\quad\times\left[\left(2J'+1\right)(2J+1)S(S+1)(2S+1)\right]^{1/2}\\&\quad\times\left[I(I+1)(2I+1)\right]^{1/2}\left\{\begin{array}{ccc} I & J' & F \\ J & I & 1\end{array}\right\}\left\{\begin{array}{ccc} J & S & N \\ S & J' & 1\end{array}\right\}.\end{aligned}\tag{B3}$$

(iv) Magnetic hyperfine interaction (II)

$$\begin{aligned}&\left\langle v'\Lambda'N'(S)J'(I)F'M_F'\right|-\sqrt{10}g_S\mu_Bg_N\mu_N(\mu_0/4\pi)T^1\left(\hat{S},C^2\right)\\&\times T^1\left(\hat{I}\right)\left|v\Lambda N(S)J(I)FM_F\right\rangle\\&=\delta_{v'v}\delta_{\Lambda'\Lambda}\delta_{N'N}\delta_{F'F}\delta_{M_F'M_F}\left(-\sqrt{30}/3\right)c_v(-1)^{J'+F+I+N}\\&\quad\times\left[\left(2J'+1\right)(2J+1)S(S+1)(2S+1)\right]^{1/2}\\&\quad\times\left[I(I+1)(2I+1)\right]^{1/2}(2N+1)\\&\quad\times\left(\begin{array}{ccc} N & 2 & N \\ 0 & 0 & 0\end{array}\right)\left\{\begin{array}{ccc} J & J' & 1 \\ N & N & 2 \\ S & S & 1\end{array}\right\}\left\{\begin{array}{ccc} I & J' & F \\ J & I & 1\end{array}\right\},\end{aligned}\tag{B4}$$

where $c_v$ characterizes the dipole–dipole interaction between $S$ and $I$.

(v) Magnetic hyperfine interaction (III)

$$\begin{aligned}&\left\langle v'\Lambda'N'(S)J'(I)F'M_F'\right|C_{vN}T^1\left(\hat{I}\right)\\&\times T^1\left(\hat{N}\right)\left|v\Lambda N(S)J(I)FM_F\right\rangle\\&=\delta_{v'v}\delta_{\Lambda'\Lambda}\delta_{N'N}\delta_{F'F}\delta_{M_F'M_F}C_{vN}\\&\quad\times(-1)^{2J+F'+I+N'+1+S}\left[N(N+1)(2N+1)\right]^{1/2}\\&\quad\times\left[\left(2J'+1\right)(2J+1)I(I+1)(2I+1)\right]^{1/2}\\&\quad\times\left\{\begin{array}{ccc} I & J & F' \\ J' & I & 1\end{array}\right\}\left\{\begin{array}{ccc} N & J & S \\ J' & N' & 1\end{array}\right\}.\end{aligned}\tag{B5}$$

(vi) Electronic spin Zeeman effect

$$\begin{aligned}&\left\langle v'\Lambda'N'(S)J'(I)F'M_F'\right|g_S\mu_BT^1\left(\hat{S}\right)\\&\times T^1_{p=0}\left(\hat{B}\right)\left|v\Lambda N(S)J(I)FM_F\right\rangle\\&=\delta_{v'v}\delta_{\Lambda'\Lambda}\delta_{N'N}\delta_{M_F'M_F}g_S\mu_BB_Z\\&\quad\times(-1)^{F-M_F+F'+2J+I+N+S}\left[(2J+1)\left(2J'+1\right)S(S+1)\right]^{1/2}\\&\quad\times\left[(2S+1)(2F+1)\left(2F'+1\right)\right]^{1/2}\left\{\begin{array}{ccc} J & S & N \\ S & J' & 1\end{array}\right\}\\&\quad\times\left\{\begin{array}{ccc} F & J & I \\ J' & F' & 1\end{array}\right\}\left(\begin{array}{ccc} F & 1 & F' \\ -M_F & 0 & M_F\end{array}\right).\end{aligned}\tag{B6}$$

(vii) Nuclear spin Zeeman effect

$$\begin{aligned}&\left\langle v'\Lambda'N'(S)J'(I)F'M_F'\right|-g_N\mu_NT^1\left(\hat{I}\right)\\&\times T^1_{p=0}\left(\hat{B}\right)\left|v\Lambda N(S)J(I)FM_F\right\rangle\\&=\delta_{v'v}\delta_{\Lambda'\Lambda}\delta_{N'N}\delta_{M_F'M_F}g_N\mu_NB_Z\\&\quad\times(-1)^{F-M_F+F+J+I}\left[(2F+1)\left(2F'+1\right)\right]^{1/2}\\&\quad\times\left[I(I+1)(2I+1)\right]^{1/2}\\&\quad\times\left\{\begin{array}{ccc} F & I & J \\ I & F' & 1\end{array}\right\}\left(\begin{array}{ccc} F & 1 & F' \\ -M_F & 0 & M_F\end{array}\right).\end{aligned}\tag{B7}$$

(viii) Stark effect

$$\begin{aligned}&\left\langle v'\Lambda'N'(S)J'(I)F'M_F'\right|-T^1_{q=0}\left(\hat{\mu}_{\mathrm{e}}\right)\\&\times T^1_{p=0}\left(\hat{E}\right)\left|v\Lambda N(S)J(I)FM_F\right\rangle\\&=\delta_{v'v}\delta_{\Lambda'\Lambda}\delta_{M_F'M_F}\mu_{\mathrm{e}}E_Z(-1)^{F'+F+1-M_F+J+I+J'+S+N}\\&\quad\times\left[(2N+1)\left(2N'+1\right)(2J+1)\right]^{1/2}\\&\quad\times\left[\left(2J'+1\right)(2F+1)\left(2F'+1\right)\right]^{1/2}\\&\quad\times\left(\begin{array}{ccc} N & 1 & N' \\ 0 & 0 & 0\end{array}\right)\left\{\begin{array}{ccc} J & N & S \\ N' & J' & 1\end{array}\right\}\\&\quad\times\left\{\begin{array}{ccc} F & J & I \\ J' & F' & 1\end{array}\right\}\left(\begin{array}{ccc} F & 1 & F' \\ -M_F & 0 & M_F\end{array}\right).\end{aligned}\tag{B8}$$

## References


[1] Chu S 1998 *Rev. Mod. Phys.* **70** 685
[2] Ketterle W 2002 *Rev. Mod. Phys.* **74** 1131
[3] Carr L D, DeMille D, Krems R V and Ye J 2009 *New J. Phys.* **11** 055049
[4] Jin D S and Ye J 2012 *Chem. Rev.* **112** 4801
[5] Hu Z K, Ke Y, Deng X B, Zhou Z B and Luo J 2012 *Chin. Phys. Lett.* **29** 080401
[6] Hudson E R, Lewandowski H J, Sawyer B C and Ye J 2006 *Phys. Rev. Lett.* **96** 143004
[7] Bishop A I, Wang L and Barker P F 2010 *New J. Phys.* **12** 073028
[8] Xia Y, Yin Y L, Ji X and Yin J P 2012 *Chin. Phys. Lett.* **29** 053701
[9] Narevicius E, Libson A, Parthey C G, Chavez I, Narevicius J, Even U and Raizen M G 2008 *Phys. Rev. A* **77** 051401(R)
[10] Rangwala S A, Junglen T, Rieger T, Pinkse P W H and Rempe G 2003 *Phys. Rev. A* **67** 043406
[11] Weinstein J D, deCarvalho R, Guillet T, Friedrich B and Doyle J M 1998 *Nature* **395** 148
[12] Sage J M, Sainis S, Bergeman T and DeMille D 2005 *Phys. Rev. Lett.* **94** 203001
[13] Liu W L, Wu J Z, Ma J, Xiao L T and Jia S T 2014 *Chin. Phys. B* **23** 013301
[14] Ni K K, *et al.* 2008 *Science* **322** 231
[15] Li J, Liu Y, Huang Y and Cong S L 2015 *Chin. Phys. B* **24** 080308
[16] Prehn A, Ibrügger M, Glöckner R, Rempe G and Zeppenfeld M 2016 *Phys. Rev. Lett.* **116** 063005
[17] Di RosaM D 2004 *Eur. Phys. J. D* **31** 395
[18] Yeo M, Hummon M T, Collopy A L, Yan B, Hemmerling B, Chae E, Doyle J M and Ye J 2015 *Phys. Rev. Lett.* **114** 223003
[19] Shuman E S, Barry J F and DeMille D 2010 *Nature* **467** 820
[20] Barry J F, McCarron D J, Norrgard E B, Steinecker M H and DeMille D 2014 *Nature* **512** 286
[21] Hemmerling B, Chae E, Ravi A, Anderegg L, Drayna G K, Hutzler N R, Collopy A L, Ye J, Ketterle W and Doyle J M 2016 *J. Phys. B* **49** 174001
[22] Truppe S, Williams H, Hambach M, Fitch N, Wall T E, Hinds E A, Sauer B E and Tarbutt M R 2016 arXiv:1605.06055
[23] Yin Y N, Xia Y, Li X J, Yang X X, Xu S P and Yin J P 2015 *Appl. Phys. Express* **8** 092701
[24] Yang R, Tang B and Gao T 2016 *Chin. Phys. B* **25** 043101
[25] Kozyryev I, Baum L, Matsuda K, Hemmerling B and Doyle J M 2016 *J. Phys. B* **49** 134002
[26] Wilkinson P G 1963 *Astrophys. J.* **138** 778
[27] Barrow R F, Bernard A, Effantin C, D'incan J, Fabre G, Hachimi AE, Stringat R and Verges J 1988 *Chem. Phys. Lett.* **147** 535
[28] Effantin C, Bernard A, D'incan J, Wannous G, Verges J and Barrow R F 1990 *Mol. Phys.* **70** 735
[29] Bernard A, Effantin C, D'incan J, Verges J and Barrow R F 1990 *Mol. Phys.* **70** 747
[30] Bernard A, Effantin C, Andrianavalona E, Verges J and Barrow R F 1992 *J. Mol. Spectrosc.* **152** 174
[31] Berg L E, Gador N, Husain D, Ludwigs H and Royen P 1998 *Chem. Phys. Lett.* **287** 89
[32] Kozlov M G, Titov A V, Mosyagin N S and Souchko P V 1997 *Phys. Rev. A* **56** R3326
[33] Nayak M K, Chaudhuri R K and Das B P 2007 *Phys. Rev. A* **75** 022510
[34] Nayak M K and Chaudhuri R K 2008 *Phys. Rev. A* **78** 012506
[35] Borschevsky A, Ilias M, Dzuba V A, Flambaum V V and Schwerdtfeger P 2013 *Phys. Rev. A* **88** 022125
[36] Vutha A C, *et al.* 2010 *J. Phys. B* **43** 074007
[37] Quemener G and Bohn J L 2016 *Phys. Rev. A* **93** 012704
[38] Kang S Y, Kuang F G, Jiang G and Du J G 2016 *Mol. Phys.* **114** 810
[39] Born M and Oppenheimer R 1927 *Ann. Phys.* **389** 457
[40] Ryzlewicz C and Torring T 1980 *Chem. Phys.* **51** 329
[41] Huber K P and Herzberg G 2005 *Molecular Spectra and Molecular Structure* IV: *Constants of Diatomic Molecules* (Van Rostrand-Reinhold)
[42] Nicholls R W 1981 *Astrophys. J. Suppl. Ser.* **47** 279
[43] Morse P M 1929 *Phys. Rev.* **34** 57
[44] Rees A L G 1947 *Proc. Phys. Soc.* **59** 998
[45] Chen T, Bu W H and Yan B 2016 arXiv:1609.07707
[46] Tarbutt M R, Sauer B E, Hudson J J and Hinds E A 2013 *New J. Phys.* **15** 053034
[47] Hudson J J, Kara D M, Smallman I J, Sauer B E, Tarbutt M R and Hinds E A 2011 *Nature* **473** 493
[48] The ACME Collaboration, *et al.* 2014 *Science* **343** 269
[49] Brown J H and Carrington A 2003 *Rotational Spectroscopy of Diatomic Molecules* (Cambridge University Press)
[50] Steimle T C, Frey S, Le A, DeMille D, Rahmlow D A and Linton C 2011 *Phys. Rev. A* **84** 012508
[51] Zare R N 1988 *Angular Momentum: Understanding Spatial Aspects in Chemistry and Physics* (New York: Wiley)
[52] Frosch R A and Foley H M 1952 *Phys. Rev.* **88** 1337
[53] Ernst W E, Kandler J and Torring T 1986 *J. Chem. Phys.* **84** 4769
[54] Curl Jr R F1965 *Mol. Phys.* **9** 585
[55] Tarbutt M R 2015 *New J. Phys.* **17** 015007
[56] Nakagawa J, Domaille P J, Steimle T C and Harris D O 1978 *J. Mol. Spectrosc.* **70** 374
[57] Steimle T C, Domaille P J and Harris D O 1978 *J. Mol. Spectrosc.* **73** 441
[58] Bernard A and Gravina R 1983 *Astrophys. J. Suppl. Ser.* **52** 443
[59] Norrgard E B, McCarron D J, Steinecker M H, Tarbutt M R and DeMille D 2016 *Phys. Rev. Lett.* **116** 063004
[60] Sushkov O P and Flambaum V V 1978 *Sov. Phys. JETP* **48** 608